Research in Astronomy and Astrophysics, 22:125017 (11pp), 2022 December https://doi.org/10.1088/1674-4527/ac9de1

Modeling and Measuring Friction of the Leighton 10 m Telescope

Yongwei Guo[1,2], David Woody[3], and Nicolas Matinez[4]

[1] Chinese Academy of Sciences South America Center for Astronomy, Camino El Observatorio 1515, Las Condes, Santiago, Chile; gyw@bao.ac.cn

[2] National Astronomical Observatories, Chinese Academy of Sciences, Beijing 100101, China

[3] California Institute of Technology, Owens Valley Radio Observatory, Big Pine, CA 93513, USA

[4] Universidad de Concepcion, Facultad de Ciencias Físicas y Matematicas, Concepcion, 403000, Chile

Received 2022 June 14; revised 2022 September 26; accepted 2022 October 10; published 2022 December 7

Abstract

Estimating and identifying friction are important aspects of simulating a mechanical drive system. Accurate friction modeling helps to improve a telescope's performance. However, the friction conditions inside are complex and hard to measure. We did simulations with mathematical transfer functions for the Leighton 10 m Telescope and employed a polyline model to identify sources of friction. We made a two-stage model for the Leighton 10 m Telescope. Based on measurements of the motor's currents and speeds, we constructed a curve containing the friction information of the transmission elements. We simulated the system using a step function input under many combinations of friction parameters. By comparing simulation results with the measured ones, we determined the various friction components. This model accurately reproduced the telescope performance including the nonlinearities.

Key words: astronomical instrumentation – methods and techniques – telescopes – methods: analytical

1. Introduction

Simulation is beneficial in optimizing the performance of complex mechanical systems. This is especially true for astronomical telescope drives that must move massive structures to track astronomical sources at one-arcsecond accuracy or better. Friction in the drive chains affects behaviors in the realistic simulation of telescopes, especially at slow tracking speeds and direction reversal. This paper describes the simulation and verification of friction forces for the Leighton 10 m diameter radio telescope operating at wavelengths as short as 300 μm.

Frictions and their identification, from the motor axis to the final load axis, are critical in making a precise simulation model. Friction affects the telescope power and is important for accurate and stable control of the telescope motion. The friction-related features are of concern to both astronomers and engineers. Precision needs to be maintained during slow sidereal tracking and rapid raster mapping. Stability in motion is required. Friction matters are challenging and changes in friction at different speeds or conditions can make it difficult to achieve stable and accurate control of the telescope pointing. Besides minimizing friction, knowing the distribution of the friction inside a telescope is beneficial.

The Leighton 10 m diameter radio telescope is well-designed and scientifically productive. The Caltech Submillimeter Observatory (CSO) has the highest precision among the seven telescopes that are part of this facility. CSO worked in the submillimeter band at Maunakea, Hawaii but is now preparing for an update and migration to the Atacama in Chile and will have a new name—Leighton Chajnantor Telescope (LCT). The other six working in the millimeter band at the Owens Valley Radio Observatory (OVRO) near Bishop, California, are more convenient to reach for testing. The future performance of the LCT, especially the rapid response for the new On-The-Fly observing mode, relies on the simulation work on the Leighton Telescope in OVRO (LTO), which depends critically on accurate mathematical models including friction identification and following possible optimizing inertias of reducers and so on. With many tests for the LTO, we found a nonlinear phenomenon in its drive system. It is hard to know which component in the telescope produces the nonlinearity because they are in daily use and cannot be disassembled. That limits us from making more detailed and precise simulation models. Studies on performances of the LCT depend on the simulation of the LTO, especially in identifying the complex friction distribution.

Why does the final output of a telescope manifest nonlinear behavior? The complex friction behavior of the telescopes was unexpected. There is a possibility that the friction nonlinearity is a result of the large 15050:1 cycloidal speed reduction in drive systems. There is also a possibility that complex manufacturing errors introduce complex inner forces that cause the friction to show nonlinearities. There may also be other unknown conditions. In making simulation models, if we simplify many sources of friction and generalize them to one source, the appearance of the combination of many sources of friction will be different from that of a single source of friction. For complex conditions, the appearance of nonlinearity may not look like standard physical friction models. So a simple general nonlinear friction model for simulations, which is compatible with both a single friction source and several combined sources, helps focus on the hidden problem from complex realities.

An accurate LTO simulation requires a good friction model. Former studies described precise models with many parameters for a single source of friction. For example, studies in literature (Tjahjowidodo et al. 2005) identified the nonlinear friction at a low speed in a motor. However, actual telescopes have many sources of friction, which run very slowly with large ratio reducers. The velocities may change constantly and continuously. The friction will change when the velocity changes. Lubrication conditions also change, which makes friction behavior even more complex. For astronomical telescopes, Rivetta & Hansen made a complex friction model with six parameters for Sloan Digital Sky Survey (SDSS) (Rivetta & Hansen 1998), and Kumar & Banavar used a complex LuGre model for the ARIES Schmidt telescope (Kumar & Banavar 2011), but it seems they are not suitable for the measured LTO performance. Even if we obtain the friction using these complex friction models, the simulation costs are high, and their internal distribution remains unknown. It is not satisfactory to use complex models if we have no idea where or why the system behaves nonlinearly.

Friction nonlinearity with speed happens mainly in two areas. One is around 0 speed. The other one is at the speed transition from low to high. The former influences telescopes' tracking and direction reversal, and the latter, which happens in LTO, is fundamental in describing the whole friction behavior.

In this paper, we try to develop a relatively simple method to identify the friction sources in LTO, and figure out their distribution as well. It not only makes the simulation faster, but also the simulation model can be a multi-stage transmission system and contain more details than before. In Section 2, we briefly introduce the nonlinear phenomena of LTO and describe the requirement for its friction model. In Section 3, we describe the method of how we identify the friction terms. We propose a polyline friction model based on multiple traditional models to solve nonlinear phenomena in telescope simulations. In Section 4, we briefly describe the model simulation and simplification for LTO. Then we show the simulation results under different friction distribution conditions. In Section 5, we compare the simulation results to the actual telescope measurements with a brief discussion. With the method, we located where the nonlinearity happened. And in Section 6, we use a more detailed and more precise model to simulate the whole model and verify the reason for the nonlinearity.

2. Nonlinear Transmission of LTO

2.1. Telescope Transmission System

A telescope transmission system often has a large speed reduction ratio so that relatively high-speed low torque servo motors can be utilized and provide a wide dynamic range from sidereal source tracking to fast slew to new sources. Figure 1 depicts a typical transmission chain such as that in LTO, which includes the motor, the coupler, the reducers, the bull gear, and so on. The bull gear fixes the reflector structure. There are two transmission chains from the two motors to this bull gear, which is typical for removing backlash in the transmission chain.

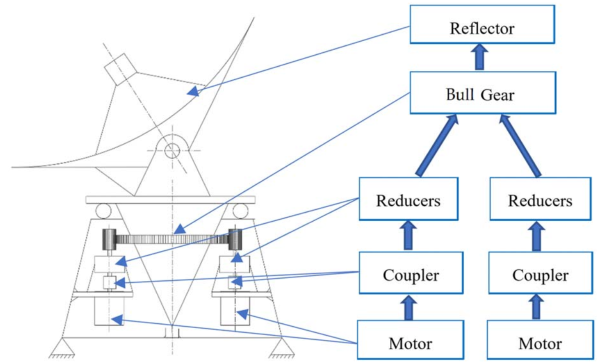

Figure 1. Typical azimuth transmission system of a telescope.

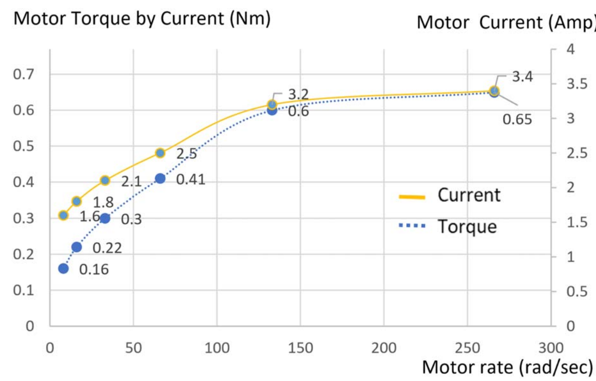

Figure 2. Chart of motor currents, torques versus rates.

2.2. Nonlinear Phenomenon

Our tests found nonlinearity in the LTO drives. The yellow curve in Figure 2 is the relationship between the motor current and rotation rate. We obtain the curve by measuring the motor currents at several constant rates and then converting them to motor torque. The current data are the average of the two motors in the telescope to simplify the analysis. After converting the curve from current (solid orange) to torque (dotted blue) according to the motor model, it becomes the curve for the motor loads versus motor rates. Because we measured the currents while the telescope runs at a constant speed, the motor load is the friction at that speed. So, we can

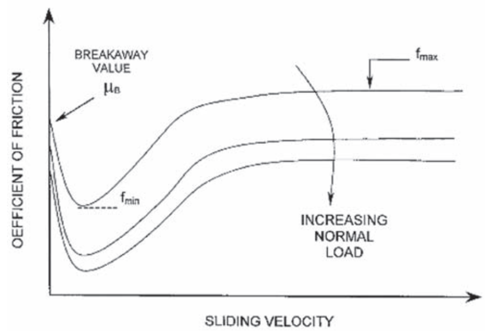

a) PTFE vs Stainless steel (Constantinou et al. 1999)

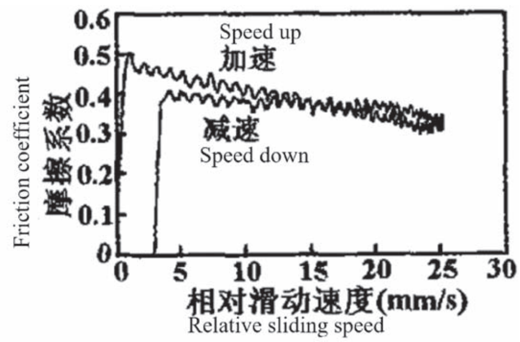

b) Steel 45 vs GCr15 steel (Chen & Shi 2002)

Figure 3. Actual relation of frictions versus velocities.

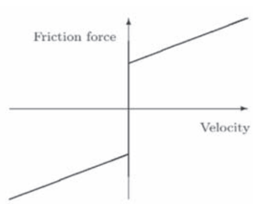

a) Coulomb model (Geffen 2009)

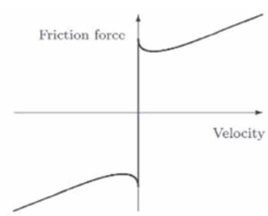

b) Stribeck model (Geffen 2009)

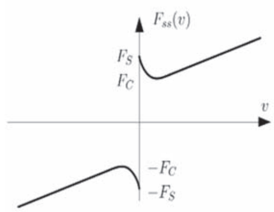

c) LuGre model (Astrom & Wit 2008)

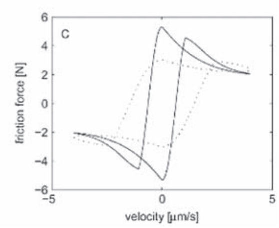

d) GMS model (Clauset et al. 2005)

Figure 4. Various low speed friction models.

conclude that the motor torque curve also characterizes the transmission friction.

If the transmission system is linear, the friction characteristic curve should increase linearly with the rate increase. From Figure 2, we can see the telescope's behavior is nonlinear.

To simulate LTO's nonlinearity, we should use a nonlinear model for friction. What model should we use, and how? We need a friction model based on actual friction phenomena which can also simulate complex nonlinear behavior.

3. Friction Models and the Simulation

3.1. Actual Friction Characteristic and Friction Models

The actual friction appears to be nonlinear when measured accurately enough. From literature (Constantinou et al. 1999; Chen & Shi 2002), we can see from the curves in Figure 3 that there is a nonlinearity when the speed increases. These curves are the friction between a single pair of surfaces. Their pressure between the surfaces is constant.

Various kinds of friction models (Clauset et al. 2005; Åström & de Wit 2008; Geffen 2009; Liu et al. 2015) have been described in the literature to make the models more precise. Figure 4 illustrates four typical traditional friction models. Except for the Coulomb model (Geffen 2009), which is too simple to exhibit details at low speed, the Stribeck (Tjahjowidodo et al. 2005; Geffen 2009), LuGre (Åström & de Wit 2008) and GMS (Clauset et al. 2005) models look complex. These models are suitable for the friction between a pair of surfaces.

When we compare Figures 3 and 4, we can see they are quite different. No matter what parameters we choose in the models drawn in Figure 4, it is hard to simulate the exact shape displayed in Figure 3.

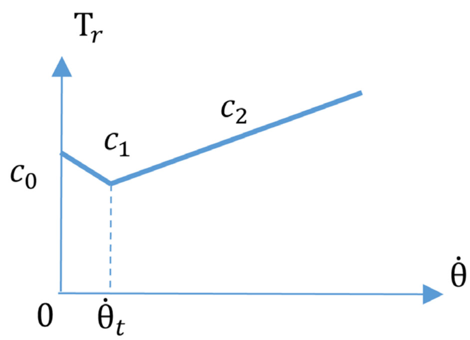

Figure 5. Profile of resistance versus velocity of the PM.

It is even harder to describe LTO using the above friction models. The curve in Figure 2 is more complex than that in Figure 3, for the outline in Figure 2 is about the characteristic of many friction pairs while that in Figure 3 is just about the characteristic of one pair.

3.2. A Simplified Friction Model—The Polyline Model

We try to use polylines to mimic the nonlinear frictions. Here we discuss rotational friction. Rotational friction is more complex than pure sliding friction under constant pressure but is more practical in a rotary machine. We denote T_r as the resisting torque of a shaft. When described as a segment of a polyline, it is

$$T_r = c_0 + c_1\dot{\theta} \quad 0 < \dot{\theta}, \tag{1}$$

where c_0 is the static friction term that resists the start of the rotation, and c_1 is the damping item. It is linear as the velocity increases.

We treat the resisting torque using polyline segments. If the lubricant condition has an abrupt change at a certain velocity, the profile of T_r turns at that velocity $\dot{\theta}_t$, that is,

$$T_r = \begin{cases} c_0 + c_1\dot{\theta}, & 0 < \dot{\theta} < \dot{\theta}_t \\ c_0 + c_1\dot{\theta} + c_2(\dot{\theta} - \dot{\theta}_t), & \dot{\theta}_t \leqslant \dot{\theta}. \end{cases} \tag{2}$$

As depicted in Figure 5, the curve of Equation (2) looks roughly similar to that in Figures 4(b) and (c). It can fit Figures 4(a) and 3(b) if we choose the proper parameters. Figure 3(a) looks more like a polyline with three segments. So, we think we can simplify the actual inner resistance by selecting the appropriate parameters of Equation (2), i.e., c_0, c_1 and c_2.

To run the simulations, while the rate is very slow, we use a line to connect 0 to friction c_0 and ignore the complex direction reversal problem for the moment. We draw it in Figure 6(b), which looks like another polyline. The velocity θ_s is small enough to not interfere with the simulation. It is mentioned in the literature (Tjahjowidodo et al. 2005) to connect 0 to the friction in the Stribeck model shown in Figure 6(a). When we consider the hysteresis like that in the GMS model, we can modify the polyline model (PM) to two segments depicted in Figure 6(c), which looks like Figure 4(d). Here we want to omit the hysteresis. So, Figure 6(b) is a simplification of Figure 6(c).

Like the other traditional friction models, the PM can be about a single friction pair. It can fit traditional nonlinear friction models to a certain degree. While $c_2 = c_1$, the PM shrinks to the Coulomb model. Unlike the models for simulating single friction pairs, the PM can also simulate complex friction phenomena, such as considering many friction pairs as one friction pair. In telescopes, the actual resisting force at the motor is a combination of many friction pairs.

3.3. Method for Building Simulation Models

We build simulation models based on the topological and physical relationships among the parts of a telescope. As a typical transmission system illustrated in Figure 1, we can regard it as a series of shaft parts connected serially. As demonstrated in Figure 7, a shaft is in a topological relation between its previous shaft and its next shaft. The thick cylinder indicates a shaft part such as a gear, a transmission shaft or something with an inertia J, while the thin cylinder indicates a virtual twist spring with a flexibility coefficient k of that shaft part. J and k can be determined by theoretical mechanics calculations.

A typical shaft has a physical relationship between the driving torque and friction. So, its dynamic and flexible equations can be expressed typically as

$$T_{\text{in}} - T_{\text{out}} - T_r = J\ddot{\theta}_{\text{out}}, \tag{3}$$

$$T_{\text{in}} = k(\theta_{\text{out}} - \theta_{\text{in}}), \tag{4}$$

in which T_{out} is the output torque of this shaft, while T_{in} is the input torque of this shaft. In addition, T_{out} is the torque coming from the next shaft, while T_{in} is the torque being applied back to the previous shaft. The T_{in} of the next shaft has a ratio to this T_{out}, that is, the transmission ratio.

We deduce the transfer function of the typical shaft with Equations (3), (4) and (2). Figure 8(a) depicts its chart, in which the friction is a PM, shown in Figure 8(b). Note that the T_{out} of this shaft is also the T_{in} of the adjacent next shaft. θ_{out} and θ_{in} are the same.

The whole telescope can be assembled by linking these units together. When this unit is a reducer, a gear or something with a transmission ratio, we should use the transmission ratio to scale the torque T_{in} and the angle displacement θ_{in} to the next shaft.

We made the telescope model for LTO with the above method. Namely, we connected the shaft models serially together. There are parallel azimuth driving chains in the telescope, which we simplify to one chain. We will discuss it in Section 4.2.

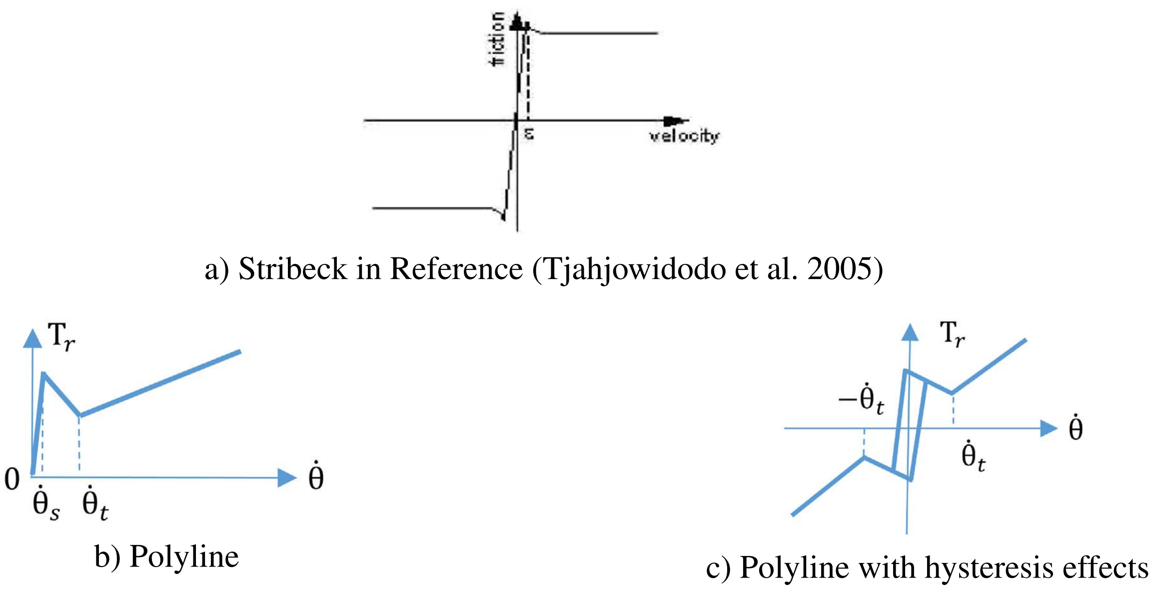

Figure 6. Simplification of friction models when the velocity passes 0.

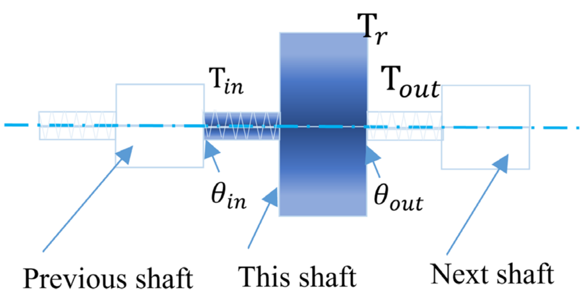

Figure 7. Typical shaft in telescopes' transmission system.

4. Simulations for LTO to Identify the Sources of Friction

4.1. Motor Loads With the Motor Rates and Currents

We will simplify the friction characteristic curve (Figure 2) of the transmission system without losing its nonlinearity. Redrawing in Figure 9, the blue fitted motor torque curve is also the friction characteristic curve of the telescope. It looks like a polyline which is a combination of two linear segments. So, we fit these two segments with straight lines. They are the red dashed lines in Figure 9. Their extensions intersect at the point (104.25, 0.5826). Next to the lines are the fitted algebraic equations.

We describe the red dashed lines as

$$T_{\rm load} = \begin{cases} 0.1447 + 0.0042x & 0 < x < 104.25 \\ 0.1447 + 0.0042 \times 104.25 + 0.000417(x - 104.25) & 104.25 \leqslant x < 266, \end{cases} \tag{5}$$

or

$$(c_0, c_1, c_2, \dot{\theta}_t) = (0.1447, 0.0042, 0.000417, 104.25). \tag{6}$$

It is the whole friction characteristic of LTO and a sum of many friction pairs inside the telescope. Because we have only one equation so far, we must append new equations and simplify the telescope model to know the exact friction distribution.

4.2. Simplify the Telescope Model

The telescope model should have enough complexity and parameters to match the measured behavior, including the friction components. A model with more transmission stages can reveal more dynamic information but may run slowly or make it difficult to determine friction components. The Leighton 10 m Telescope has a driving transmission chain similar to Figure 1. There are several transmission stages and a structure of two copies of the chains operating in parallel driving the common bull gear.

As illustrated in Figure 10(a), we simplify the transmission system model into two parts by rates. They are the high rate part and the low rate part. Each is like the typical shaft drawn in Figure 7. In the high rate part, there is the coupler and the input shaft of the reducer, while in the low rate part, there are the output shaft of the reducer and the bull gear fixed with the reflector.

We accumulate resistances on the low rate part up to be the resistance $T_{\rm rl}$ and accumulate resistances on the high rate part up to be the resistance $T_{\rm rh}$. The simulation model should still be

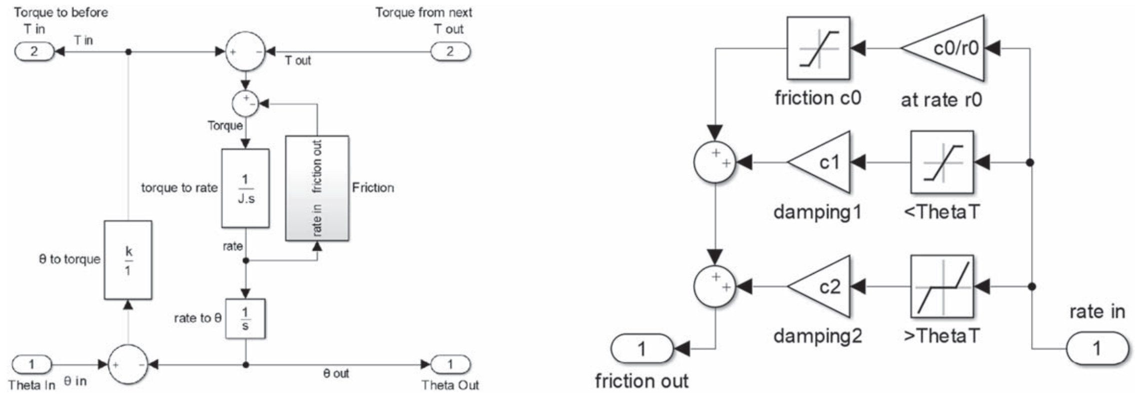

a) typical shaft model b) polyline friction model chart

Figure 8. Transfer function chart of a typical shaft.

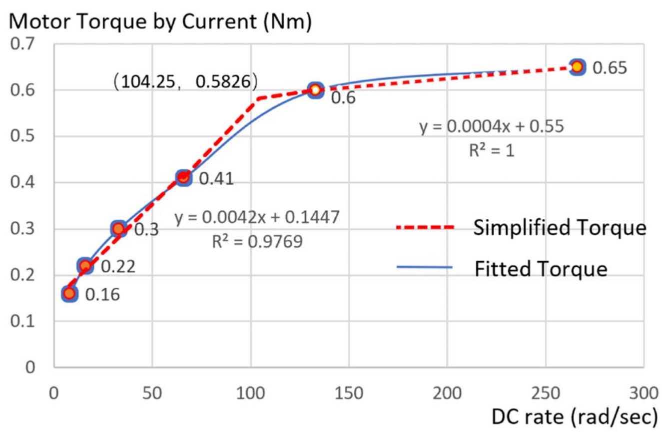

Figure 9. Fit of the motor torque to the polyline.

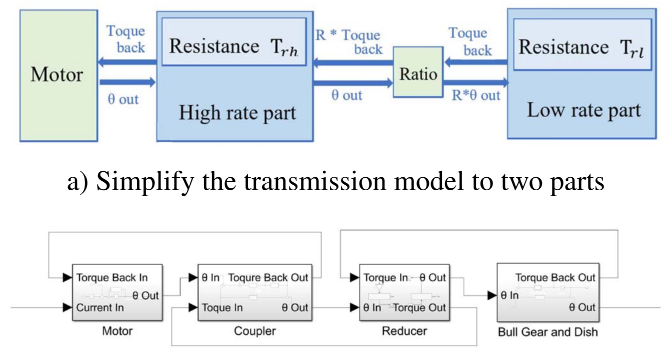

a) Simplify the transmission model to two parts

b) Simulation diagram for LTO

Figure 10. Transmission system model.

linear, for we describe these nonlinear resistances as a series of straight polylines. Because of the reducer's torque ratio R for the telescope, while resisting torques are transferred and summed to the motor shaft, the load torque on the motor $T_{\rm load}$ will be

$$T_{\rm load} = T_{\rm rh} + RT_{\rm rl}. \tag{7}$$

Note that the inertia of the low rate part is driven by two forces from two parallel drive chains to produce the correct system frequency in the simulation. From Figure 1, we can see there are two chains of reducers for driving the bull gear. This is a traditional way of removing the backlash. We simplify the model to one chain in Figure 10(a) to make it easy to measure. So here, T only corresponds to one chain for the simplified model. The actual friction on the bull gear is $2T_{\rm rl}$.

Simulation model for the LTO is depicted in Figure 10(b). Parameters such as inertias and masses are derived from the telescope structure models in the simulation, while other parameters, such as motor and reducer, are from the manufactures. We list some parameters in Table 1.

Table 1
Some Parameters of the Leighton 10 m Telescope

	Inertia (kg m^2)	K (N m rad^{-1})	Torque Ratio
Low rate part	116711	8.97×10^7	1/15050
High rate part	0.002	2.11×10^4	

4.3. Solving the Friction Equation

We assume the break points in the polyline occur in just one transmission component. Break points at different velocities would rarely overlap because of the large speed reduction between components. We only need to use the PM in one part to mimic nonlinearity. Among the other parts, we can use the linear model, such as the simple traditional Coulomb model. Here, we suppose two conditions, one is that the nonlinearity occurs in a low speed component, the other is that the nonlinearity occurs in a high speed component. By simulation in Section 4.5, we can determine where the nonlinearity happens.

If we assume that the PM is at the high speed component, denoting $T_{\rm rl}$ as the resisting torque at the low speed component and $T_{\rm rh}$ as the resisting torque at the high speed component, then,

$$T_{\rm rl} = c_{0l} + c_{1l}x \qquad 0 < x \leqslant 266$$
$$T_{\rm rh} = \begin{cases} c_{0h} + c_{1h}x & 0 < x < 104.25 \\ c_{0h} + c_{1h}104.25 + c_{2h}(x - 104.25) & 104.25 \leqslant x \leqslant 266 \end{cases}, \tag{8}$$

in which x is the velocity at the motor's output shaft. Here, $T_{\rm rl}$ is the equation of the traditional Coulomb model, while $T_{\rm rh}$ is that of the PM model. From Equations (7) and (5), and the piecewise function Equation (8), there is

$$\begin{cases} c_{0h} + Rc_{0l} = c_0 \\ c_{1h} + Rc_{1l} = c_1 \\ c_{2h} + Rc_{1l} = c_2. \end{cases} \tag{9}$$

Here we suppose $c_{0h} \geqslant 0$ and $c_{0l} \geqslant 0$ because the static friction should not be less than 0 here. We also suppose $c_{2h} \geqslant 0$ because the friction might decrease when the rate increases locally, but as a whole, the friction should increase while the rate increases. In this way, we estimate the range of c_{0h} and Rc_{1l} by Equation (9). When $Rc_{1l} \in [0, c_1]$, $c_{1h} \geqslant 0$, and when $Rc_{1l} \in [c_1, \infty]$, $c_{1h} < 0$. Though there are five unknown parameters with only three equations, we get the following relations

$$\begin{cases} c_{0h} \in [0, c_0] \\ Rc_{1l} \in [0, c_1] \cup (c_1, \infty) \\ Rc_{0l} = c_0 - c_{0h} \\ c_{1h} = c_1 - Rc_{1l} \\ c_{2h} = c_2 - Rc_{1l}. \end{cases} \tag{10}$$

If we suppose the PM is at the low speed component, in the same way, we get the following equation group as

$$\begin{cases} c_{0h} = [0, c_0] \\ c_{1h} = [0, c_1] \cup (c_1, \infty) \\ Rc_{0l} = c_0 - c_{0h} \\ Rc_{1l} = c_1 - c_1h \\ Rc_{2l} = c_2 - c_{1h}. \end{cases} \tag{11}$$

4.4. Adding Dynamic Equations

Here we add equations containing dynamic information. The equations above are static because they are from the measurements under constant speed. There is insufficient information to solve the static equations directly by themselves. We introduce the step function $h(t)$, which relates the dynamic information of the telescope's transmission system. It is also easy to measure experimentally. That is,

$$h(t - \tau) = \begin{cases} 1 & 0 < t < \tau \\ 0 & \tau \leqslant t \end{cases}. \tag{12}$$

While we feed the function $h(t-\tau)$ to the motor, the telescope should output the information relative to the internal friction distribution.

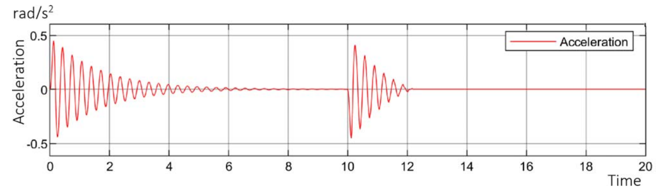

Figure 11. Typical response of the function $h(t - \tau)$.

4.5. Simulations for Different Conditions

The simulation is a process of evolution under physical principles over time. It will mimic how these objects move under specific conditions in a computer. We simulated the situation when the input is $266h(t-10)$ rad s^{-1} and obtained the reflector's rotation acceleration responses. A typical response looks like that in Figure 11. The horizontal axis is time in s, while the vertical axis is acceleration in rad s^{-2}. From $0 \sim 10$ s, it is the response of the start. From $10 \sim 20$ s, it is the response of the stop.

Interestingly, the response looks like a damped oscillation. The fact that the function $h(t-\tau)$ made the motor stop instantly makes it look like a resonant mode response. Here the damping of the system is nonlinear, so the system is not easy to analyze using standard resonant mode response. Mathematical transfer functions make the simulation easy to run for different cases and conditions. Furthermore, the input function can be other mathematical curves as well. It is more common for simulations to be run in the time domain than in the frequency domain.

Table 2 lists the simulation results for the case that the PM is in the high speed component, while Table 3 lists the corresponding results for the low speed component. They are cropped from 10 to 13 s to clearly show the stopping process. The parameters are from low to high or vice versa, which mean these response curves vary with these parameters nearly continuously. These tables show the relationship between the simulation curves and the friction parameters. The curve has sufficient parameters or degrees of freedom to correspond to these friction parameters. A set of parameters will relate to a unique response curve and vice versa. With these tables, we can find the main variation between simulation results and friction parameters, and under which parameters the simulation result best matches the test described in Section 5.

Table 2
Responses if PM is at High Rate Part

	c_{0h}=0.0 Rc_{0l}=0.1447	c_{0h} = 0.04 Rc_{0l}=0.1047	c_{0h} = 0.07 Rc_{0l}=0.0747	c_{0h}=0.11 Rc_{0l}=0.0347	c_{0h} = 0.144 Rc_{0l}=0
Rc_{1l}=0 c_{1h}=0.0042 c_{2h}=0.0004					
Rc_{1l}=0.0001 c_{1h}=0.0041 c_{2h}=0.0003					
Rc_{1l}=0.0002 c_{1h}=0.0040 c_{2h}=0.0002					
Rc_{1l}=0.0003 c_{1h}=0.0039 c_{2h}=0.0001					
Rc_{1l}=0.0004 c_{1h}=0.0038 c_{2h}=0.0					

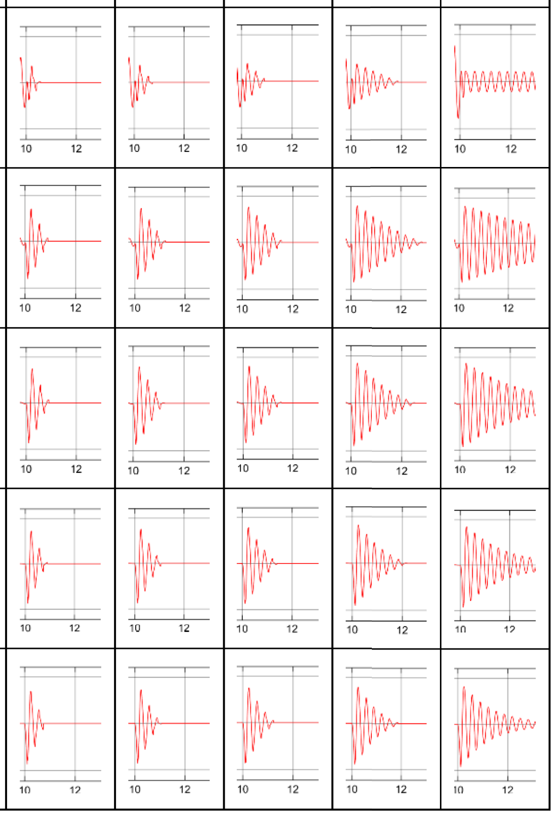

Table 3
Responses if PM is at Low Rate Part

	c_{0h}=0 Rc_{0l}=0.1447	c_{0h}=0.04 Rc_{0l}=0.1047	c_{0h}=0.07 Rc_{0l}=0.0747	c_{0h}=0.11 Rc_{0l}=0.0347	c_{0h}=0.1447 Rc_{0l}=0.0
c_{1h}=0 Rc_{1l}=0.0042 Rc_{2l}=0.0004					
c_{1h}=0.0001 Rc_{1l}=0.0041 Rc_{2l}=0.0003					
c_{1h}=0.0002 Rc_{1l}=0.0040 Rc_{2l}=0.0004					
c_{1h}=0.0003 Rc_{1l}=0.0039 Rc_{2l}=0.0002					
c_{1h}=0.0004 Rc_{1l}=0.0038 Rc_{2l}=0.0					

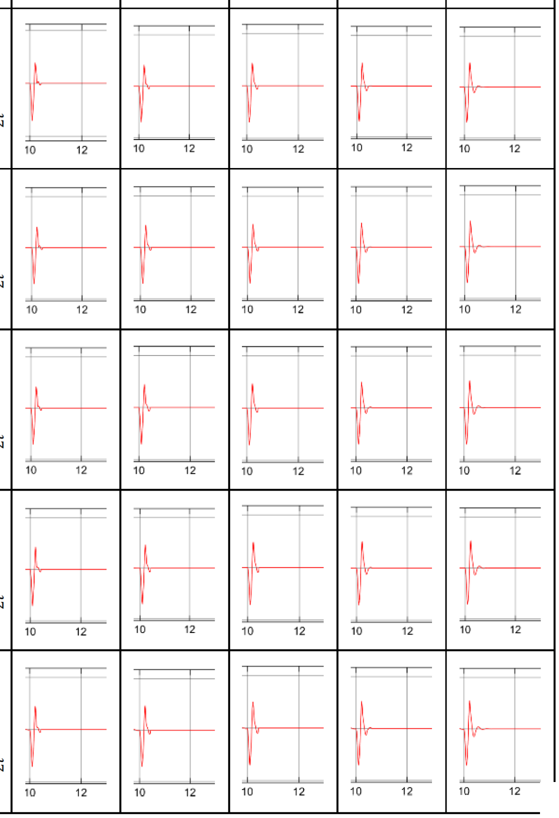

5. Parameters Determined by Test

We did the test on Leighton Telescope #2 in OVRO. An accelerometer was attached to the reflector's support structure to provide faster readout of its motion and aid in the determination of the telescope's response time to the stop command. The accelerometer does not need precision calibration for this analysis.

We measured the responses while the telescope suddenly stopped, which takes about 2 s from full speed to stop. You can see the accelerometer waveforms in Figure 12. All simulations of the PM in the low speed component are much shorter than 2 s or even 1 s from Table 3, which means it is very unlikely that the PM is in the low speed component.

5.1. Resulting Parameters

Among the simulations with the PM in the high speed component, shown in Table 2, we can see some results similar to the test. In Figure 13, we scale the vertical axes to similar sizes for easy comparisons. The fact that the test responses are overlapping indicates the test is repeatable. We can see the sampling frequency is higher than the Nyquist Limit. Though there are high-frequency noises in the test results, they are still reliable.

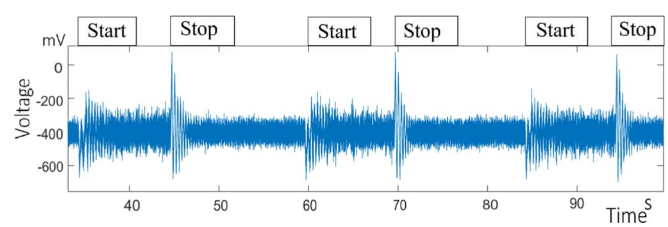

Figure 12. Accelerometer's responses while starting and stopping.

When $c_{0\mathrm{h}} = 0.11$ and $Rc_{1l} = 0.0003$, the resistances at the high and low speed components are respectively

$$T_{\mathrm{rh}} = \begin{cases} 0.11 + 0.0039x & 0 < x < 104.25 \\ 0.50615 + 0.0001x & 104.25 \leqslant x \leqslant 266 \end{cases}$$
$$RT_{\mathrm{rl}} = 0.0347 + 0.0003x \qquad 0 < x \leqslant 266, \qquad (13)$$

in which x is the velocity at the motor.

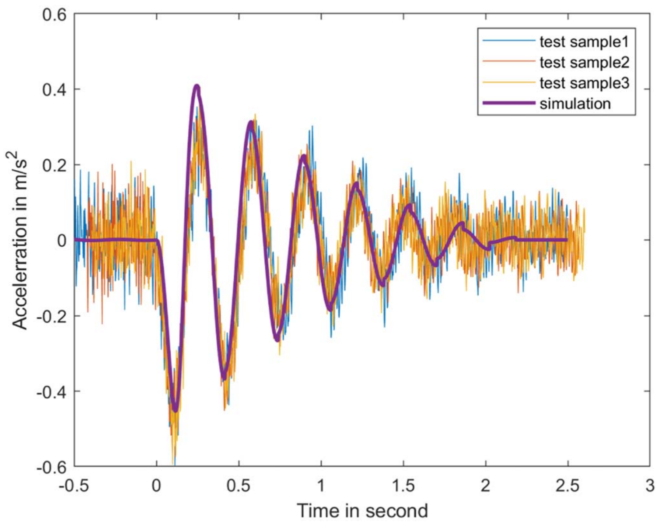

Figure 13. Stopping curve for the test, simulation and their coherence.

5.2. Internal Friction Graph and Verification

The frictions look normal both at the high and low speed components. They have non-zero friction parameter c_0 and damping c_1. We can see the friction characteristic curves in Figure 14. With the friction parameters we have solved above, we constructed the model of the telescope drive system. Figure 15 plots simulated and measured currents. The agreement is very good and verifies the validity of the friction model and parameter estimation.

6. Discussion and Possible Improvements

6.1. Discussion

We conclude that the nonlinear PM is at the high speed end of the drive system. It implies that the working conditions of the telescope are complex and that a possible lubricant change might happen inside the reducer, around the coupler or the reducer's input shaft at the rate of about 1000 rpm (that is 104 rad s^{-1}). Determining the physical reasons will require further study.

We cannot use traditional friction models for every component in LTO's simulation here. The friction characteristic curve T_{rh} displayed in Figure 14(a) cannot be produced by the friction models listed in Figure 4. The break point of the curve is at a relatively fast rotation rate. It is difficult to explain by existing higher-order damping, such as by viscous friction, because of the slow increase in friction at high speeds. It is in the high speed section and not the stiction of the gearbox at slow speeds.

We use a two-stage transmission simulation model to handle the friction distribution. It is more precise and accurate than a one stage model and still has a short execution time. Although the friction distribution we obtained inside the telescope is approximate, it may help identify the source of the nonlinear friction.

It would be valuable to further this study to improve the identification accuracy. At very slow rates, Stribeck effects may

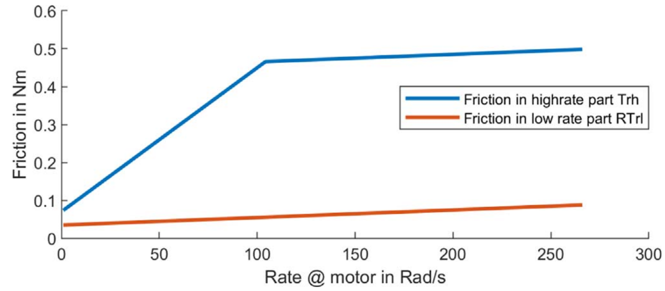

Figure 14. Friction graph.

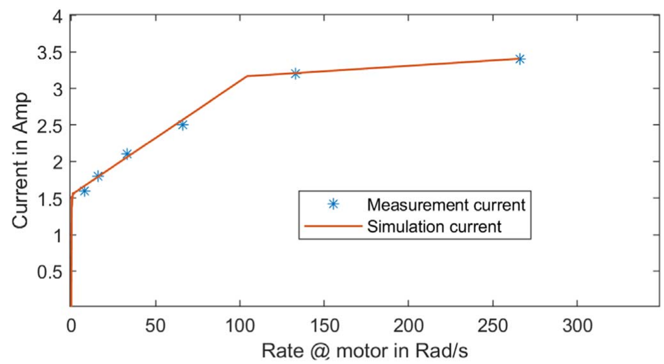

Figure 15. Simulation current and test current.

occur, though we did not see them. This may be because the rate is not slow enough when sampling the currents. More precise current measurements and putting more accelerometers on the telescope should improve the model accuracy. It is important to make more measurements at very slow speeds to capture any nonlinearities that will be important for slow sidereal tracking and direction reversal.

Simulations are playing an increasingly important role but the friction models remain complicated and poorly determined. Measuring friction characteristic curves under different loads and speeds is fundamental for nonlinear simulations and performance improvements.

6.2. Model Improvement

It would be very useful to know the cause of the nonlinearity. Here we use a quadratic curve to fit the measured friction in Figure 16 to improve the model. With the same method as that in Section 4, we fit the shape and its equation as demonstrated in Figure 16.

Leaving RT_{rl} unchanged, the sum of RT_{rl} and T_{rh} should be equal to the total friction load equation in Figure 16 by Equation (7). So, we get T_{rh} as expressed in Equation (14)

$$\begin{aligned} T_{\mathrm{rh}} &= 0.1007 + 0.0047x - 1.147 \times 10^{-5}x^2 \\ RT_{\mathrm{rl}} &= 0.0347 + 0.0003x \qquad 0 < x \leqslant 266. \end{aligned} \tag{14}$$

Figure 17 features the friction graph, in which T_{rh} is a parabola. From Wen & Huang (2008), we found nonlinear

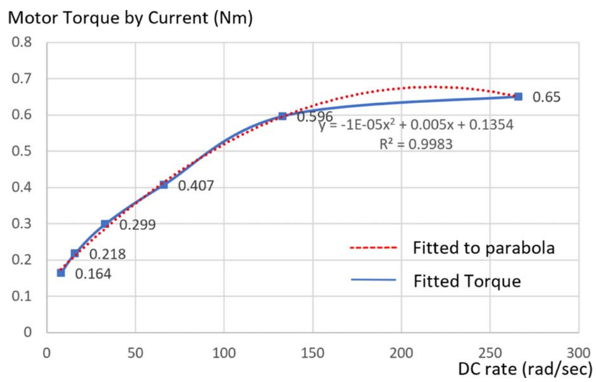

Figure 16. Fit of the friction contour to a parabola.

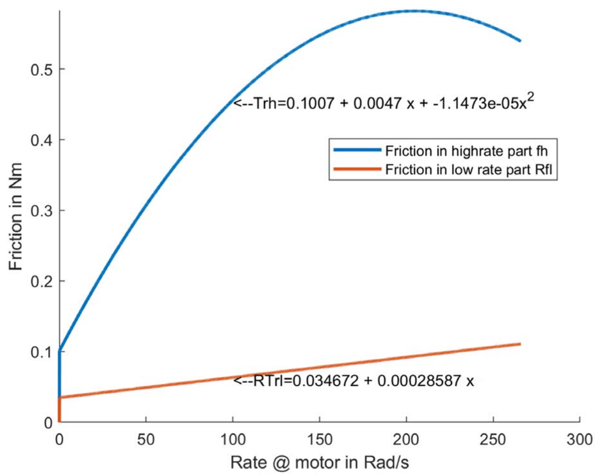

Figure 17. Friction graph.

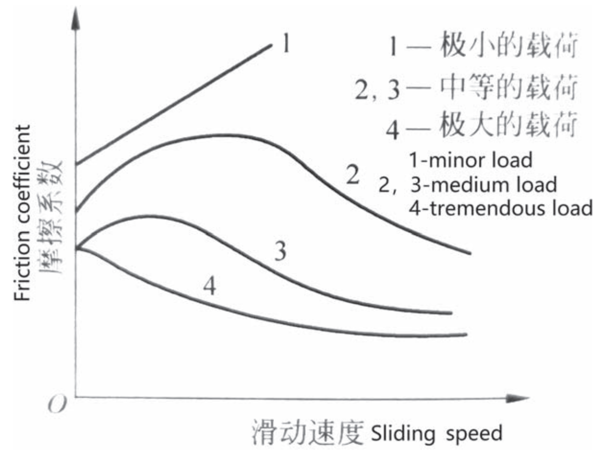

Figure 18. Friction graph (adapted from Wen & Huang 2008).

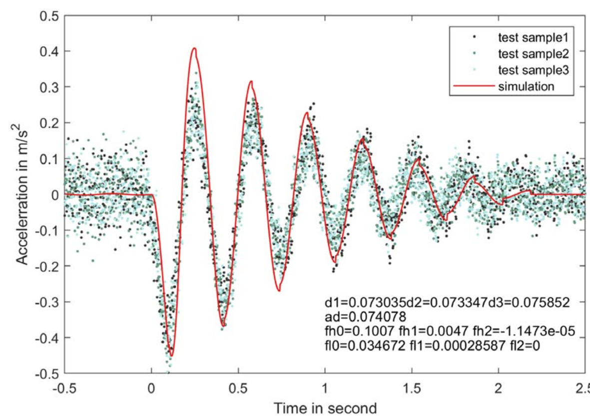

Figure 19. Stop curve of the test, the simulation and their coherence.

behavior under different loads, as affirmed in Figure 18. Upon comparing these two figures, we can see that T_{rh} looks like the left half of the 2nd curve. The fitted quadratic looks very similar to the medium load case in Figure 18.

With the frictions described as in Equation (14), the simulated stop curve in Figure 19 looks like Figure 13.

To refine the parameters and improve the agreement between the simulation curve and the stopping vibration curve, we define a general distance $d = \mathrm{Stdev}(\mathrm{MinDist})$, such that,

$$\mathrm{MinDist} = \mathrm{Min}\sqrt{(V_s - V_t)^2 + [k(t_s - t_t)]^2}. \tag{15}$$

We search the parameters of Equation (14) by changing them a little to find the minimum d value. V and t in Equation (15) are the acceleration value, and the time of the sampled points and the curve respectively. k is a scale parameter to balance the different units between time and acceleration. At last, we get the refined parameters as expressed in Equation (16),

$$\begin{aligned} T_{\mathrm{rh}} &= 0.13 + 0.0042x - 1.147 \times 10^{-5}x^2 \\ RT_{\mathrm{rl}} &= 0.00537 + 0.000786x \qquad 0 < x \leqslant 266, \end{aligned} \tag{16}$$

and their curves plotted in Figure 20.

With the refined friction model shown in Figure 20 or Equation (16), we simulate the stop curve in Figure 21. The agreement is better than that for the PM displayed in Figure 13. The difference between Figures 13 and 19 is minor and they are different from Figure 21. This may be because we judge the agreement in Figures 19 and 13 by vision instead of calculation in Figure 21.

We have simulated the current curve in the refined friction model as shown in Figure 22. The agreement looks better than that in Figure 15. The model can be further improved by measuring the currents for many different cases at both high and very low speeds. If the new sample points are still on the

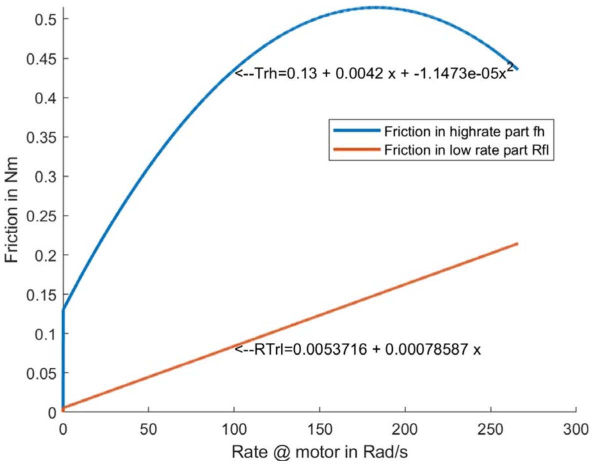

Figure 20. Friction graph.

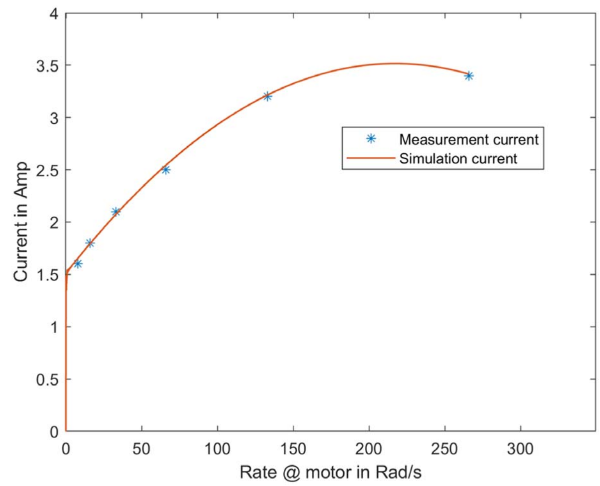

Figure 22. Simulation current and test current.

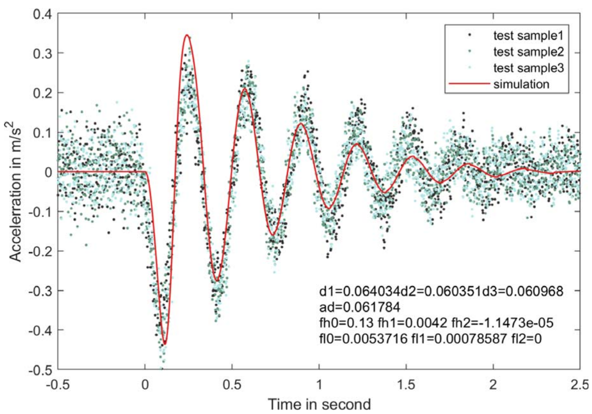

Figure 21. Stop curve of the test, the simulation and their coherence.

simulation curve, it will verify our assumption that the heavy load at the high speed component produces the nonlinearity of the telescope friction. This would suggest we investigate the use of a different speed reducer for the future LCT.

7. Conclusions

We simulated the nonlinearity of the Leighton 10 m Telescope with a polyline friction model. We detected its inner friction distribution by comparing the measured stopping curves to the simulations. The PM is simple, flexible in application and can be applied in systems where lubrication conditions change. The method describes the fully operational telescope and does not require measuring the individual drive system components.

The PM serves as a rough starting point for the simulation. Later a more precise traditional nonlinear model can be developed for a more detailed study. It is fundamental for the simulation to be evaluated at very low and very high speeds.

With the friction parameters determined in this paper, the simulation model has satisfactory precision and running speed for simulating the control performance of the Leighton 10 m Telescope. We deduced that the nonlinearity happens in the high speed components under heavy load. This will help in the process of updating the Leighton Chajnantor Telescope.

Acknowledgments

This work is sponsored (in part) by the Chinese Academy of Sciences (CAS) through a grant to the CAS South America Center for Astronomy (CASSACA) in Santiago, Chile. We thank Isu Ravi for providing the current detections and Michael Stramenga for the comments on the model. We thank Drs. Zhong Wang, James Lamb, Cong Xu, Yanfeng Dai, Morgan Catha and Piaoran Liang for helpful comments and discussions. We also thank Dr. Hairen Wang for calculating some mechanical parameters of the Leighton 10 m Telescope.

References

Åström, K. J., & de Wit, C. C. 2008, IEEE Contr Syst Mag, 28, 101
Chen, G. X., & Shi, X. Y. 2002, LubEn, 3, 44
Clauset, A., Newman, M. E. J., & Moore, C. 2005, ITAC, 50, 1883
Constantinou, M. C., Tsopelas, P., Kasalanati, A., et al. 1999, Property Modification Factors for Seismic Isolation Bearings, http://hdl.handle.net/10477/813
Geffen, V. 2009, A Study of Friction Models and Friction Compensation, http://mate.tue.nl/mate/pdfs/11194.pdf
Kumar, T. S., & Banavar, R. N. 2011, IFAC Proc. Volumes, 19, 980
Liu, Y. F., Li, J., Zhang, Z. M., et al. 2015, MecSc, 6, 15
Rivetta, C. H., & Hansen, S. 1998, Proc. SPIE, 3351, 466
Tjahjowidodo, T., Bender, F. A., & Brussel, H. V. 2005, IFAC Proc. Volumes, 38, 554
Wen, S. Z., & Huang, P. 2008, Principles of Tribology (3rd ed.; Beijing: Tsinghua Univ. Press)